Extreme Water Levels for Australian Beaches using Empirical Equations for Shoreline Wave Setup

J. G. O'Grady[1], K. L. McInnes[1], M. A. Hemer[2], R. K. Hoeke[1], A. Stephenson[3] and F. Colberg[4].

[1]CSIRO Ocean and Atmosphere, Melbourne, Australia. [2]CSIRO Ocean and Atmosphere, Hobart, Australia. [3]CSIRO DATA61, Melbourne, Australia. [4]BOM, Melbourne, Australia.

Corresponding author: Julian O'Grady (julian.ogrady@csiro.au)

Key Points:

- Quantile comparison of shoreline wave setup equations *vs* measurements demonstrates their ability to predict the highest measured levels
- New ~30yr hindcasts of shoreline wave setup are used with a storm-tide hindcast to predict the extreme mean total water level climate
- Beach slope is shown to be important to the contribution of waves to mean total water levels

Keywords

Shoreline wave setup; mean total water level; extreme water level; empirical regression analysis; hindcast

Abstract

Empirical equations for wave breaking and wave setup are compared with archived shoreline wave setup measurements to investigate the contribution of wind-waves to extreme Mean Total Water Levels (MTWL, the mean height of the shoreline), for natural beaches exposed to open ocean wind-waves. A broad range of formulations are compared through linear regression and quantile regression analysis of the highest measured values. Shoreline wave setup equations are selected based on the availability of local beach slope data and the ability of the quantile regression to show a good representation of the highest measured levels. Wave parameters from an existing spectral wave hindcast are used as input to the selected equations and are combined with a storm-tide time series to quantify the relative contribution of shoreline wave setup to the extreme MTWL climate along Australian beaches. A multi-pass analysis is provided to understand the ability to capture the shoreline wave setup estimates with and without considering beach slope. The national scale analysis which does not include beach slope indicates there are multiple contributing factors to MTWL. Examples are provided at two locations of differing local beach slope to show the importance of including local beach slope in determining the contribution of waves to MTWL. A tool is in development for further investigation of wave setup for Australian beaches.

Plain Language Summary

Understanding how high ocean water levels can reach up the coast is important for designing coastal protection from coastal inundation and erosion. This is particularly important as climate change affects wind and weather conditions and sea-level rise with the subsequent modification to the occurrence of the largest storm-driven water levels. While the height of storm-driven water levels are well understood for protected harbors and estuaries, new research is providing estimates of how high water levels can reach for coastlines exposed to dangerous wave/surf conditions. This study uses mathematical model simulations spanning ~30 years of historical water levels and ocean waves. Statistical analysis is performed to determine how high the largest storm events will likely reach on natural sandy beaches directly exposed to large wave/surf conditions. The study demonstrates that estimates are very sensitive to local beach characteristics. The paper presents the science behind a tool (which is in development) to allow further investigation of the contribution of waves/surf to the highest water levels for individual beaches.

1. Introduction

Understanding the climate of extreme water levels is important for coastal protection, particularly as climate change affects wind and weather conditions and sea-level rise, subsequently modifying extreme water levels (McInnes et al., 2016; Vitousek et al., 2017; Vousdoukas et al., 2018; Wong et al., 2014). The contributing processes to water level extremes include ocean-basin scale steric and barotropic sea levels, astronomical tide, atmospheric forced coastal storm surge, wind-wave driven wave setup and wave runup, each of which can occur in isolation or coincidentally. Wave setup is defined as the increase in the mean water level across the surf zone due to the presence of waves and can be a major contributor to inundation for coastlines exposed to large waves (O'Grady & McInnes, 2010). Wave setup provides the mean contribution of waves to the shoreline water level. Wave runup provides the further contribution of waves to shoreline water levels by including higher water levels which are only reached by the highest swash motions up the beach face. In this manuscript the term Mean Total Water Level (MTWL) is used to indicate the mean height of shoreline water level with the inclusion of wave setup, juxtaposed to the Total Water Level (TWL) which has been used to indicate the shoreline height which is exceeded at higher percentiles (e.g. 2% exceedance percentile or maximum height) of the water level with inclusion of wave runup (e.g. Serafin et al., 2017).

There is increased interest in the contribution of waves to extreme water levels given recent storm events, for example the Sydney June 2016 event (Mortlock et al., 2017) and reports on the compounding effect of sea level rise on wave-driven extreme events (Melet et al., 2018; Rueda et al., 2017; Vitousek et al., 2017). There is also increasing availability of regional and global hindcast and reanalysis datasets of the various contributing factors to extreme water level, and a requirement to provide these data through climate services (Le Cozannet et al., 2017). Accurate predictions of the contribution of waves to MTWL (or TWL) are dependent on the local beach slope (Nielsen, 1988). The lack of systematic beach-profile measurements makes it difficult to accurately predict the contribution of waves to MTWL at the global or national scale (Turner et al., 2016). There are also few observations of the contribution of waves to MTWL, particularly in Australia, to validate the model prediction of extreme wave conditions (Hanslow & Nielsen, 1993; Nielsen, 1988).

Australia has a wide diversity of coastal beaches, including fringing reef coastlines and rocky platforms, each of which produce a different shoreline wave effect (Buckley et al., 2018; Merrifield et al., 2014; Power et al., 2018). As first step to identifying the contribution of waves to extreme water levels, this paper will focus on estimates for natural sandy beaches directly exposed to open ocean wind-waves only. Estimates will be provided for the entire coast for continuity in the first pass analysis, which will include cliffed coastlines and coastlines behind fringing reefs. Therefore, local scale interpretation of the national maps should consider the nearshore bathymetry and coastal geomorphology. This initial effort to include waves will also limit the focus on the shoreline wave setup, which is the maximum value of the wave setup water surface across the surf zone and is measured as the time-averaged height of the shoreline. The analysis of wave runup, measured as higher percentile shoreline heights, is not presented in detail here to narrow the focus of the study to wave setup. Wave runup has related processes and empirical equations to shoreline wave setup and is as important as wave setup to extreme sea level hazards. The remainder of this paper is organised with a review of previous studies on extreme water levels (Section 2), shoreline wave setup equations (Section 3) and description of the data and models used in this study (section 4). Results are presented (Section 5) reanalysing historic field measurements, then providing national maps of shoreline wave setup and MTWL as a broad scale analysis followed by examples for Australian beaches. Discussion and conclusions are provided (Section 6) with the aim of developing a tool to access the return level curves for MTWL for each Australian Beach.

2. Extreme water level climate

The contributors to extreme water level, (e.g. MTWL or TWL), depend on where the water level is measured (Figure 1) and the statistical measure of the water level, (e.g. mean or 98th percentile value). The different terms for the contributors are summarised in Table 1. This definition of MTWL as used in this paper is along the lines of the TWL but without wave runup heights at the beach as described in Serafin et al., (2017).

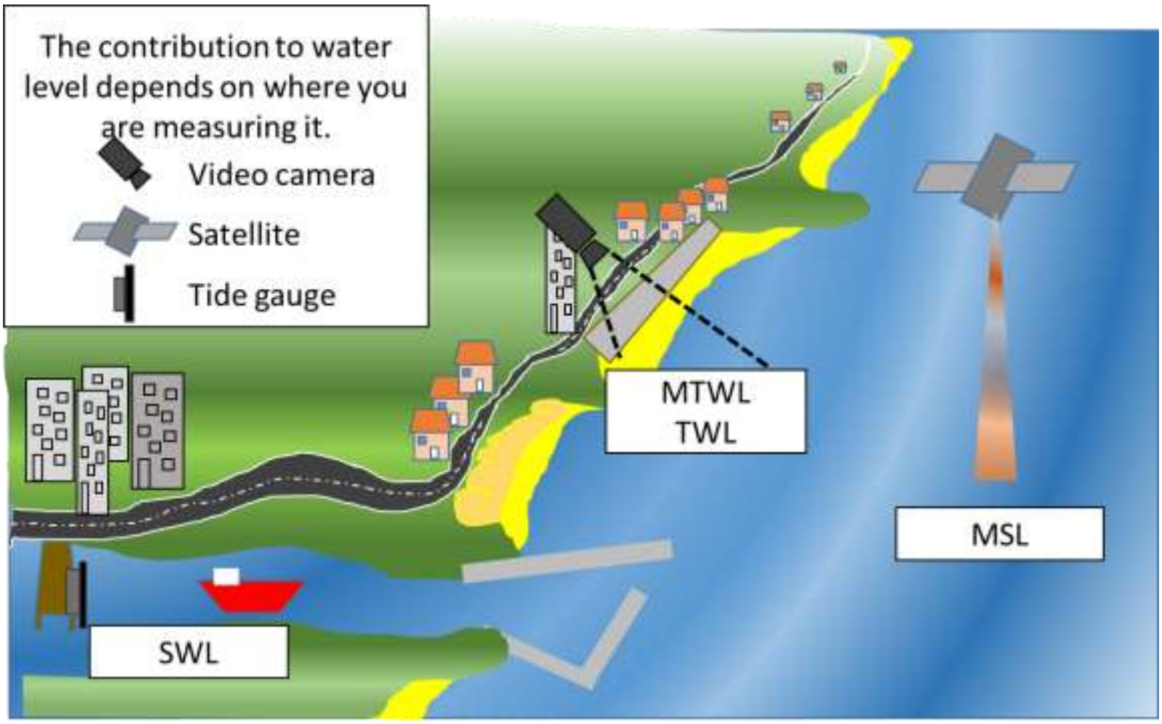

Figure 1 Diagram showing the location of different measurements of extreme water level. Vertical level abbreviations are described in Table 1.

Figure 2 shows the cross-shore beach profile of the contributors to MTWL and TWL. Above a physical datum, the still water level (SWL) is defined as the time-averaged water level (on the order of 6 minutes to one hour) due to astronomical tide, atmospheric driven water level (surge) and steric and barotropic effects. For an open ocean beach, the SWL is assumed to be horizontal across the surf zone (Figure 2). Wave setup is defined as the increase in the time-averaged (on the order of 15 minutes to one hour) water level due to the presence of waves. The horizontal wave setup water surface increases shoreward across the surf zone (Figure 2). The maximum value of wave setup, which occurs at the beach face is defined as the shoreline wave setup and it corresponds to the MTWL (Table 1). Shoreline wave setup is measured as the time-averaged swash line height relative to the SWL. It is assigned the term shoreline wave setup $\bar{\eta}_s$, where η is the free water surface relative to the SWL, the over-bar denotes the time-average and the subscript s indicates that it is at the location of the shoreline.

*Table 1 Description of water level terms. In each column, a bold '**X**' indicates the important measured component(s) which differentiates the water level term from the water level terms in the other columns. See Figure 2 for graphical representation.*

Description	Mean sea level	Still water level	Mean total water level	Total water level
Abbreviation	MSL	SWL	MTWL	TWL
Commonly Measured by a	Satellite altimeter	Tide gauge	Video camera	Video camera
location	Open ocean	Sheltered harbor	Beach shoreline	Beach shoreline
Includes:				
-Wave runup				**X**
-Wave setup			**X**	x
-Atmospheric surge		**X**	x	x
-Astronomical tide	x	**X**	x	x
-Barotropic	**X**	x	x	x
-Steric	**X**	x	x	x
Typical sampling statistic	Interannual mean	6-60 min mean	15-60 min mean	15-60 min 98th percentile
How is the important component (**X**) resolved?	Low-pass filter	Harmonic tidal analysis and high-pass filtered storm surge	SWL at the tide gauge subtracted from MTWL	SWL at the tide gauge subtracted from TWL

Studies have investigated the contribution of waves to TWL at a global and national scale (Melet et al., 2018; Serafin et al., 2017). In Australia, studies have investigated the extreme water level climate considering tide and storm surge contributions, using tide gauge measurements and hindcast simulations that represent the SWL at the coast (Colberg et al., 2019; Haigh, MacPherson, et al., 2014; Haigh, Wijeratne, et al., 2014). In this study a historical dataset of wave setup is generated from a numerical spectral wave hindcast (Durrant et al., 2013). Empirical shoreline wave setup equations are then used to estimate the contribution of wave setup to the extreme MTWL climate along the ocean coast of Australia.

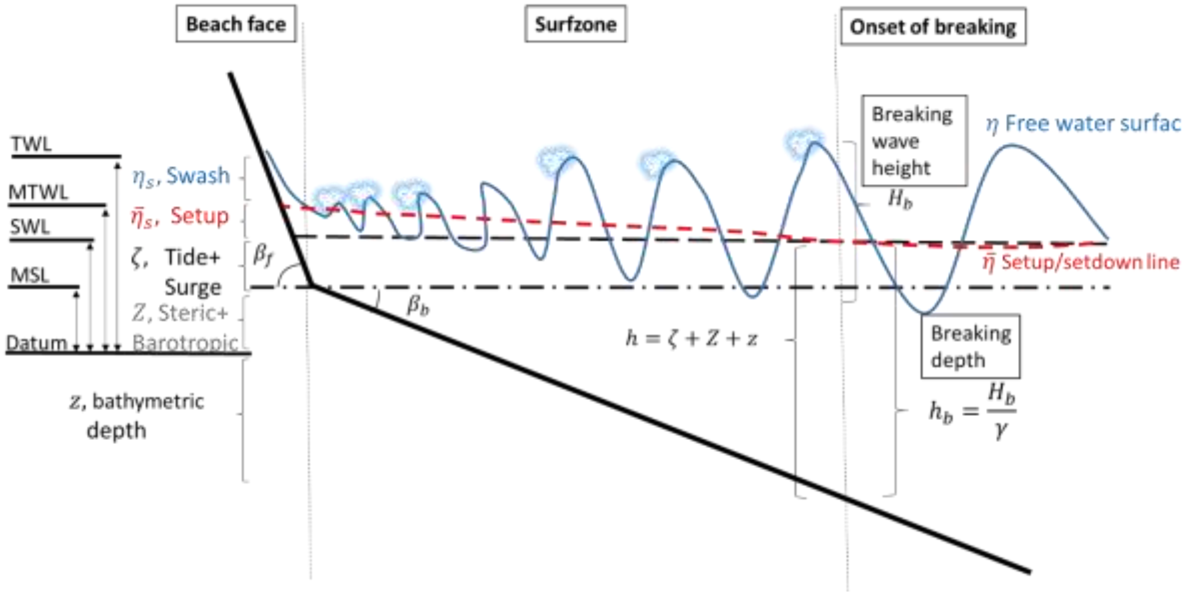

Figure 2 Diagram of wave setup in extreme water levels. Blue curved line is the instantaneous free water surface wave η, red dashed curve is the time-averaged wave setup and set down water surface $\bar{\eta}$, black dashed line is the still water level (SWL), black dot-dashed line is the mean sea level (MSL) and black solid line is the beach bathymetric profile z. Vertical water level abbreviations (MSL, SWL, MTWL and TWL) are described in Table 1. H_b is the height of the waves at the onset of breaking.

3. Shoreline wave setup equations for natural sandy beaches

The mathematical theory of wave setup, represented by partial differential equations (PDEs) for the wave stress gradient (Longuet-Higgins & Stewart, 1964) has been used to predict wave setup across the surf zone, e.g. by solving the numerical approximations of the PDEs, as done in the SWAN model (Battjes and Janssen, 1978; Holthuijsen, 2007). The PDE in the cross-shore direction can be simplified with the generalised assumption that across the surf zone the ratio of wave height to depth (γ, breaking parameter) remains constant and waves are non-dispersive in the shallow water (wave group speed equals the phase speed). This simplification results in the horizontal gradient in wave setup being roughly proportional to the bathymetric gradient (Longuet-Higgins & Stewart, 1964). The PDE of wave setup can then be simply integrated horizontally across the surf zone to work out the value of wave setup at the shoreline (Dalrymple & Dean, 1991; Holthuijsen, 2007),

$$\bar{\eta}_s = \alpha\gamma H_b \ , \qquad 1$$

where H_b is the height of the waves at the onset of breaking and α is the constant value of 0.31 in Holthuijsen, (2007) and varies with γ in Dalrymple and Dean, (1991). The challenge with this equation is that H_b is difficult to measure in the field, and there is no analytical equation relating H_b to deep water wave theory characteristics. Furthermore the assumption on a constant breaking parameter across the surf zone is questionable (e.g. Apotsos et al., 2008) .

Shoreline wave setup $\bar{\eta}_s$ has been measured (as the mean elevation at the shoreline relative to the SWL) by pressure sensors, resistance wires, photogrammetry (video cameras) and remote SONAR or LIDAR ping-return range finder sensors (Brodie *et al.*, 2015; Gourlay, 1992;

Stockdon *et al.*, 2006 and references therein). Accompanying this, regression analysis has shown relationships between empirical parametrisations and measurements of shoreline wave setup, wave and beach characteristics. The simplest regression parametrisation relates $\bar{\eta}_s$ as proportional to deep water wave height, which is commonly referred to as the 'rule of thumb' (Guza & Thornton, 1981). More involved empirical relationships have presented a dependence on the surf similarity or Iribarren number (Bowen et al., 1968; Nielsen, 1988), which compares the bathymetric (β_b in Figure 2) or beach slope (β_f in Figure 2) to the wave steepness ratio and has been used to predict breaking type, surging, plunging or spilling breakers (Iribarren & Nogales, 1949),

$$\xi = \beta \left(\frac{H}{L}\right)^{-n}, \qquad 2$$

where β represents the bathymetric or beach slope, H is the wave height and L is the wave length. The exponent n is most commonly assigned the value of 0.5, but 0.3 has been used (Gourlay, 1992). Using Equation 2, regression analysis has shown,

$$\bar{\eta}_s \propto \alpha H \xi, \qquad 3$$

where α is the slope parameter of the zero crossing regression analysis. Differences in the empirical formulation of γ, ξ and $\bar{\eta}_s$ throughout the literature arise because the wave parameters can represent bulk parameters, such as significant wave height (H_0), peak period (T_p) measured in the field, or represent individual waves in flume studies to better align with linear wave theory. The wave parameters can also represent deep water waves or the waves at the onset of breaking.

We note that the main difference between the mathematical solution to $\bar{\eta}_s$ in Equation 1 and the empirical regression parametrisation in Equation 3 is that the former is formulated on the basis of the bathymetric slope (β_b) across the surf zone , i.e. radiation stress from wave shoaling (setdown) and depth-induced breaking, and the latter is dependent on beach slope (β_f), i.e. wave swash which is influenced by the asymmetric swash/runup effect on the beach slope (Gourlay, 1992; Holman & Sallenger, 1985). This is important when considering that the measured mean shoreline level (shoreline wave setup) is a function of both wave breaking induced setup across the surf zone, and a component of time-averaged asymmetric swash effect. Having noted this, numerical coupled wave-hydrodynamic models have been tuned to match both the empirical models (Equation 3) and measurements and account for the combined bathymetric depth-induced breaking induced setup and beach swash slope effect (Ji et al., 2018; Stockdon et al., 2014).

An approach which could be considered to have separated the contribution of bathymetric depth-induced breaking and beach swash processes, though not explicitly indicated, is the spectral partitioning analysis of the swash height (Buckley et al., 2018; Stockdon et al., 2006, 2014). The bathymetric depth-induced breaking effect could be largely (but not exactly) attributed to spectral significant height of frequencies lower than the chosen threshold, e.g. 0.05Hz (infragravity waves) and the beach face swash effect to significant height of frequencies higher than that threshold (incident waves) considering the studies such as Guza & Thornton, (1982); Symonds & Bowen, (1984). Here, the data presented in Stockdon et al., (2006) indicates that the measured significant swash height contributions from the infragravity partition (bathymetric depth-induced breaking) and incident partition (beach face swash) are of similar magnitude for the chosen partition frequency (0.05Hz).

Other studies have added an extra wave setup term to the parameterisation of wave runup to improve their regression analysis of wave runup, but do not directly attribute this extra parameter to either the depth-induced breaking or a mean component of the asymmetric beach face swash effect (Atkinson et al., 2017; Holman, 1986). Nevertheless, from multiple lines of evidence, regression analysis against measurements and numerical model simulations has shown the parametrisation of the combined $\bar{\eta}_s$ from bathymetric depth-induced breaking induced setup and beach swash effect to be proportional to the wave height (at breaking or in deep water) multiplied by the surf similarity parameter (Equation 3).

Few field measurements of shoreline wave setup exist at coastal locations in Australia (Nielsen, 1988; Nielsen & Hanslow, 1991). In the subsequent sections of this study we test empirical equations for wave breaking and wave setup (Gourlay, 1992) with setup measurements using video cameras from beaches in the Northern Hemisphere (Stockdon et al., 2006) to understand the ability of the different empirical formulations to predict shoreline wave setup. These equations are then compared to measurements in Australia of swash transgressions past an array of stakes utilising the assumption that the shoreline follows a Rayleigh distribution (Nielsen & Hanslow, 1991). Spectral wave hindcast fields (Durrant et al., 2013) are provided as input to the selected empirical equations and combined with a time series of regional ocean model system (ROMS) modelled SWL (Colberg et al., 2019) to resolve the contribution of shoreline wave setup to the extreme MTWL climate at Australian beaches.

4. Measurements, model data and methods

4.1. Observations

Observations of waves, beach slopes and shoreline wave setup were sourced from the video camera experiments presented by Stockdon et al., (2006). Deep water wave length is estimated with the equation,

$$L_0 = gT_0^2/(2\pi) \; , \qquad 4$$

where L_0 is the deep water wave length and T_0 is the deep water peak period.

Additional Australian field data of waves and setup were sourced from Nielsen & Hanslow, (1991). Here, shoreline wave setup was measured by counting the swash transgression past a number of stakes. Assuming swash waves follow a Rayleigh distribution, $\bar{\eta}_s = 0.89L_{zwm}$, where $L_{zwm} = C_1(H_{0,rms}L_0)^{0.5}$, C_1 is the best-fit parameter and $H_{0,rms}$ is the root-mean-squared wave height. By convention, wave heights are assumed to obey the Rayleigh distribution in deep water, indicating that, $H_0/H_{0,rms} = \sqrt{2}$ (Ji et al., 2018). Here the L_0 was calculated with Equation 4 with T_0 equal to the deep water significant wave period T_s. The non-directional Sydney wave-rider buoy measurement for the study period (1988-1990) indicate $H_0/H_{0,rms} \approx \sqrt{2}$ and $T_p/T_s \approx 1.2$.

Observed tide gauge SWL return levels were sourced from Haigh *et al.*, (2014a). These values were used for validation of the extreme value distributions fitted to the ROMS hindcast data.

Beach slope observations were selected from the long term beach profile monitoring on the New South Wales (NSW) coastline (Turner et al., 2016, http://narrabeen.wrl.unsw.edu.au/). The mean intertidal beach slope for the five transects was calculated as slope between the linear interpolated zero and 2m water elevations which correspond to the range of the intertidal zone and is relative to the Australian Height Datum (AHD)(Turner et al., 2016).

4.2. Numerical hindcast data

Time series of SWL from computed storm surge and tide (storm-tide) were sourced for a string of points around the coastline at 10km intervals from a ROMS model simulations (Colberg et al., 2019). The ROMS model was run from the start of 1981 to the end of 2013 on a ~5km resolution regular grid and was forced with hourly ~38km grid resolution Climate Forecast System Reanalyses (CFSR) atmospheric data. The ROMS hindcast is used in this study because it uses the same atmospheric reanalysis as the wave model and because of the availability of end of 21st century climate simulations for future research into the changes in extreme water level climate. Extreme SWL distributions fitted to a modelled hindcast using Danish Hydraulic Institute's (DHI) Mike-21 flexible mesh model were sourced from Haigh *et al.*, (2014a) at the same string of points around Australia as the ROMS simulations. The Mike-21 model was run from 1949 to 2009 on a unstructured grid, with a maximum resolution of ~10km at the coast and forced by 6 hourly ~250km grid resolution National Center for Environmental Prediction (NCEP) atmospheric data. The Mike-21 distributions were used to reference the 1-year ROMS SWL to the Australian height datum (AHD), using the method described in Haigh, Wijeratne, et al., (2014). For each corresponding ROMS coastal point, the nearest grid point in a depth of at least 20 m was identified in a Wave Watch three (WWIII) spectral wave hindcast (Durrant et al., 2013) which was run on a ~7km grid. At these locations, the significant wave height and peak wave period is extracted for the years 1981 to 2013 inclusive. Empirical wave setup was calculated at all coastal WWIII points for every output time step. A time series of MTWL is computed by adding the hourly time series of empirical wave setup $\bar{\eta}_s$ to the hourly time series ROMS SWL.

4.3. Extreme value analysis

The annual maximum method (AMM) is used to evaluate extreme MTWL, shoreline wave setup, and SWL, where the highest value each year is selected to create time series of yearly annual maximum values. For longer return periods, the annual recurrence interval (RI) can be written in terms of the probability of exceedance (EP) (Pugh, 1996),

$$RI(EP) = -1/\log(EP) \qquad 5$$

This approximation, which is used for plotting in R statistical software package ismev (Coles, 2001), can be used with the Gumbel distribution quantile function (cumulative distribution function) to predict the water level return interval extreme value distribution (EVD),

$$z(RI) = \mu - \lambda \log\left(\frac{1}{RI}\right), \qquad 6$$

where z is the water level return level corresponding to either the shoreline wave setup ($\bar{\eta}_s$), SWL or MTWL, μ is the location parameter, and λ is the scale parameter fitted to the hindcast AMM values. The Gumbel EVD was preferred over EVDs that include an additional shape parameter, to avoid including the assumption that the ~30 year dataset is long enough to also correctly represent this additional parametric term of asymptotic curvature at higher RI (Arns et al., 2013). R's ismev package is used to fit Equation 6 to the AMM hindcast data to identify the maximum likelihood estimates of the μ and λ parameters and their covariance matrix (COV). The 5 and 95th percentile uncertainty curves are calculated as,

$$z_u(RI) = \mu - \lambda \log\left(\frac{1}{RI}\right) \pm 1.96se(RI), \qquad 7$$

where $se(RI)$ is the standard error calculated as,

$$V(RI) = [1, \exp(-1/RI)] \times COV \times [1, \exp(-1/RI)]^T,$$
$$se(RI) = \sqrt{V}, \quad 8$$

and V is the matrix multiplication of the exceedance probabilities with the covariate matrix (COV) from the model fit. The Gumbel parameters in Equation 6 were first calculated from the AMM of the hourly time series for each coastal point in the ROMS SWL simulations, then from the hourly time series for the corresponding WWIII point for two shoreline wave setup ($\bar{\eta}_s$) equations, and finally from the hourly time series of the ROMS SWL added to each of the hourly shoreline wave setup equations to create the MTWL time series. The one year and 100-year RI return levels were then calculated with Equation 6 for the SWL, shoreline wave setup and MTWL using the corresponding Gumbel parameters.

5. Results

5.1. Validation of empirical equations for shoreline wave setup

In this section an empirical relationship is sought to describe shoreline wave setup from the list the equations in Table 2 that have been used in regression analyses with empirical measurements of shoreline wave setup (Stockdon et al., 2006). Some of the equations are more related to wave breaking than shoreline wave setup (e.g. Van Dorn, 1978). The order of the equations in the table starts with a single dependence of deep water significant wave height H_0 then includes beach slope β_f and the wave steepness $(H/L)^{-n}$ parameters from Equation 2. Beach slope in the empirical dataset changes on the time scale of a single tidal cycle and with seasonal storm climate. Only a mean value of beach slope is available for some Australian beaches, so the mean beach slope at each location $\bar{\beta}_f$ (in the empirical dataset) is included in the regression analysis. A zero crossing regression is used to fit the data, with the consideration that a wave with zero height will result in zero wave setup.

The Pearson correlation coefficient, r, is squared to represent the coefficient of determination and is used to indicate the proportion, or percentage, of variance in the dependant variable (measured $\bar{\eta}_s$) that is predictable from the independent variable(s) (H_0, β_f and L_0). On its own, the deep water significant wave height rule of thumb equation captures 30% of the variance of shoreline wave setup (Table 2). Including the wave steepness parameter with H_0 and $n = -1/2$ explains a further 8% of the variance, while the equation with an optimised regression value of $n \approx -1/3$,similar to Van Dorn (1978), explains a further 12%. Including the mean location beach slope $\bar{\beta}_f$ with H_0 explains a further 12%, and $\bar{\beta}_f$ with H_0 and the wave steepness parameter explains a further 8%. Including the time varying value of beach slope typically explains 4% more than mean location beach slope. The root mean square error (RMSE) improves from a value of 0.25 to 0.20m through including more parameters in the equations.

At best, the analysis shows that the empirical equations can capture 54% of the variance. So to summarise, it appears that the significant wave height explains the largest portion of the variance, followed by beach slope and then the wave steepness term. The remaining variance could be accounted for by camera and tide gauge SWL datum measurement error, unresolved parameterisation of the effect of local sea vs remote swell, wave direction, embayment characteristics, beach porosity and water table effects (Gourlay, 1992).

Table 2 Empirical model zero crossing regression parameters α and n and goodness of fit parameters. The r^2 values indicates the percentage of the total variation in the measurements can be explained by the linear relationship between empirical model and the Stockdon et al., (2006) *measurements. The row values in bold are from* (Stockdon et al., 2006)*. Coloured text corresponds to Figure 3, Figure 6 and Figure 7.*

regression Form $\bar{\eta}_s$	Appears in	regression parameters α	n	Pearson r^2	RMSE (m)
αH_0	**Guza & Thornton 1981**	**0.31**	**-**	**0.299**	**0.253**
$\alpha \bar{\beta}_f H_0$	-	3.71	-	0.434	0.231
$\alpha \beta_f H_0$	-	3.61	-	0.466	0.229
αH_0^n	-	0.40	0.61	0.317	0.235
$\alpha \bar{\beta}_f H_0^n$	-	4.65	0.66	0.430	0.217
$\alpha \beta_f H_0^n$	-	4.56	0.63	0.456	0.214
$\alpha H_0 \left(\frac{H_0}{L_0}\right)^{-\frac{1}{2}}$	-	0.03	-	0.38	0.224
$\alpha \bar{\beta}_f H_0 \left(\frac{H_0}{L_0}\right)^{-\frac{1}{2}}$	Nielson 1988	0.35	-	0.42	0.223
$\alpha \beta_f H_0 \left(\frac{H_0}{L_0}\right)^{-\frac{1}{2}}$	**Stockdon et al 2006**	**0.35**	**-**	**0.485**	**0.213**
$\alpha H_0 \left(\frac{H_0}{L_0}\right)^{n}$	-	0.06	-0.36	0.416	0.218
$\alpha \bar{\beta}_f H_0 \left(\frac{H_0}{L_0}\right)^{n}$	Gourlay 1992	1.06	-0.28	0.499	0.206
$\alpha \beta_f H_0 \left(\frac{H_0}{L_0}\right)^{n}$	-	0.92	-0.30	0.543	0.200
$\alpha H_0 \left(\frac{H_0}{L_0}\right)^{-\frac{1}{3}}$	Van Dorn 1978	0.07	-	0.415	0.218
$\alpha \bar{\beta}_f H_0 \left(\frac{H_0}{L_0}\right)^{-\frac{1}{3}}$	-	0.81	-	0.492	0.207
$\alpha \beta_f H_0 \left(\frac{H_0}{L_0}\right)^{-\frac{1}{3}}$	-	0.79	-	0.540	0.200

Quantile regression analysis (Q-Q) plots for a selection of equations in Table 2 are compared to the empirical measurements to examine how well the fitted linear regression parameters (Table 2) represent the highest measured levels of the distribution (Figure 3). For the equations not considering local beach slope (Figure 3a), the basic rule of thumb relationship of $\bar{\eta}_s = 0.31H_0$ best captures the highest measured levels and should be considered when using empirical equations for extreme value analysis where the beach slope is unknown. With the inclusion of beach slope, the relationships including wave height and wave steepness are better at resolving the highest measured levels (Figure 3b). The challenges with building a national shoreline wave setup hindcast, is that there is limited beach slope data (Turner et al., 2016), which limits how well we can represent the population of extremes ($\bar{\eta}_s$ and MTWL) and how the event timing of the wave extremes with surge and tide will play out. Therefore an initial first-pass national analysis is presented in the next section, which uses the simple rule of thumb to capture the extremes where the beach slope is unknown.

The analysis in the next section is also presented for a higher-order second-pass beach scale analysis for three beach slope categories; gentle, moderate and steep based on the distribution of the empirical dataset (Stockdon et al., 2006). The moderate beach slope of 0.087 is based on the mean beach slope in the empirical dataset. We note that the slope of the regression equations (α) (Table 2) without a beach slope are equivalent to the corresponding equation with a beach slope $\bar{\beta}_f \approx 0.083$ to 0.086. To represent a wide range of beach slope categories within the measured profiles, a gentle beach slope was assigned the 5th percentile 0.023 and the steep beach slope was assigned the maximum value 0.16 from the empirical dataset (Stockdon et al., 2006). The maximum value was chosen because beach slopes in Australia have been measured larger than 0.16 (Turner et al., 2016).

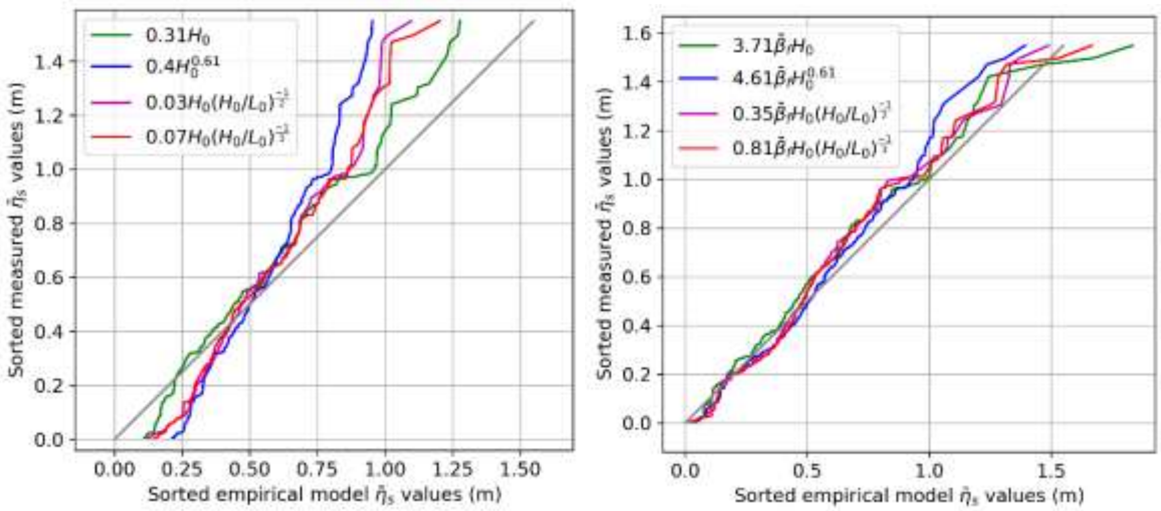

Figure 3 Empirical quantile-quantile plots. The 491 sorted measured values (Stockdon et al., 2006) *are plotted against the sorted empirical model estimates to show the comparison of climate population highest measured levels. See Table 2 for time series model comparison.*

Repeating this regression analysis with the 38 measurements for the Australian beaches (Nielsen & Hanslow, 1991) yielded a similar scale parametrisation (α) but with a reduced goodness of fit for both the rule of thumb $\bar{\eta}_s = \alpha H_0$ ($\alpha = 0.29, r^2 = 0.25, RMSE = 0.334$) and the equation including wave steepness $\bar{\eta}_s = \alpha H_0 (H_0/L_0)^{-1/3}$ ($\alpha = 0.07, r^2 = 0.25, RMSE = 0.3$). Including beach slope showed a reduced scale parameterisation (α) and reduced goodness of fit for both the rule of thumb $\bar{\eta}_s = \alpha \bar{\beta}_f H_0$ ($\alpha = 2.8, r^2 =$

$0.45, RMSE = 0.39$) and the equation including wave steepness $\bar{\eta}_s = \alpha \bar{\beta}_f H_0 (H_0/L_0)^{-1/3}$ ($\alpha = 0.71, r^2 = 0.47, RMSE = 0.36$) for the Australian beaches. Therefore there is reasonable agreement between the northern hemisphere video camera-based measurements (Stockdon et al., 2006) and the Australian transgressions past an array of stakes measurements which have reduced measurement sample and assumptions on the Rayleigh distribution (Nielsen & Hanslow, 1991).

5.2. Extreme value analysis results

5.2.1. ROMS SWL validation

Computed annual return levels (Equation 6) from ROMS SWL (Colberg et al., 2019) hindcast simulations and extreme value analysis are compared to detrended measurements at 30 validation sites in Haigh *et al.*, (2014) using their method for adjusting for the AHD. We note that this method to adjust for AHD removes any validation of storm-tide at the 1-year return level and improves the comparison at higher return intervals (10- 50- and 100-year) by removing any issues in the modelled tidal range or storm surge magnitude captured in 1-year return level from the higher return levels. The limitations with the ROMS and Mike-21 modelled tidal range and storm surge magnitudes are provided in the cited source literature (Colberg et al., 2019; Haigh, Wijeratne, et al., 2014). The Haigh *et al.*, (2014) study presented results for a generalised extreme value (GEV) fit but indicates the preferred distribution was the Gumbel (GUM) which provided similar results to GEV r-largest method. Table 3 compares the GEV fitted using AMM 10-, 50- and 100-year measured return levels to the ROMS modelled GUM values. The model comparison performs poorly at the Wyndham tide gauge where there are complex storm-tide conditions, so is removed from the comparison. The average differences across the 29 sites (excluding Wyndham) are 0.03 m larger than the Haigh study, which is understandable given they used GEV fits with a limiting shape parameter for the comparison. The difference between the models is small considering Mike-21 is run for a period around double that of the ROMS simulations, while the ROMS simulation have twice the grid resolution of the Mike-21 model at the coast and a much higher temporal and spatial atmospheric forcing data. This perhaps suggest higher temporal and spatial resolution storm-tide modelling can offset the shortcoming of shorter duration modelling to estimate extreme values.

Table 3 Comparison of the SWL 10-,50- and 100- year tide-gauge measured GEV using a AMM and ROMS model predicted GUM using a AMM return levels for 2010 (relative to m AHD).

	10-year			50-year			100-year		
Site Name	Meas.	Pred.	Abs.	Meas.	Pred.	Abs.	Meas.	Pred.	Abs.
Point Lonsdale	1.18	1.16	0.02	1.27	1.28	0.01	1.32	1.33	0.01
Geelong	1.02	0.99	0.03	1.08	1.10	0.02	1.11	1.15	0.04
Williamstown	1.03	1.05	0.02	1.10	1.19	0.09	1.13	1.24	0.11
Fort Denison	1.35	1.30	0.05	1.46	1.36	0.10	1.55	1.38	0.17
Newcastle	1.25	1.21	0.04	1.34	1.27	0.07	1.42	1.30	0.12
Brisbane	1.65	1.64	0.01	1.69	1.69	0.00	1.70	1.71	0.01
Bundaberg	2.02	1.96	0.06	2.11	2.04	0.07	2.17	2.08	0.09
Mackay	3.75	3.61	0.14	3.96	3.68	0.28	4.12	3.71	0.41
Townsville	2.40	2.34	0.06	2.62	2.43	0.19	2.80	2.48	0.32
Cairns	1.96	1.89	0.07	2.08	1.97	0.11	2.14	2.00	0.14
Darwin	1.66	1.53	0.13	1.92	1.70	0.22	2.13	1.77	0.36
Milner Bay	3.97	3.98	0.01	4.08	4.05	0.03	4.15	4.09	0.06
*Wyndham	4.12	3.77	0.35	4.33	3.77	0.56	4.58	3.78	0.80
Broome	5.25	5.27	0.02	5.35	5.41	0.06	5.38	5.47	0.09
Port Hedland	3.76	3.65	0.11	4.04	3.76	0.28	4.30	3.81	0.49
Carnarvon	1.29	1.14	0.15	1.43	1.18	0.25	1.53	1.20	0.33
Geraldton	1.06	0.91	0.15	1.19	1.02	0.17	1.27	1.06	0.21
Fremantle	1.11	0.98	0.13	1.27	1.07	0.20	1.39	1.11	0.28
Bunbury	1.18	1.04	0.14	1.37	1.15	0.22	1.52	1.20	0.32
Albany	1.01	1.00	0.01	1.06	1.06	0.00	1.08	1.09	0.01
Esperance	1.18	1.18	0.00	1.24	1.28	0.04	1.26	1.33	0.07
Thevenard	1.91	1.82	0.09	2.05	1.97	0.08	2.13	2.03	0.10
Port Lincoln	1.67	1.46	0.21	1.86	1.57	0.29	1.99	1.62	0.37
Port Pirie	2.61	2.41	0.20	2.86	2.63	0.23	3.03	2.73	0.30
Port Adelaide outer	2.39	2.17	0.22	2.62	2.31	0.31	2.78	2.37	0.41
Port Adelaide	2.26	2.05	0.21	2.44	2.18	0.26	2.56	2.24	0.32
Victor Harbour	1.51	1.43	0.08	1.61	1.54	0.07	1.67	1.59	0.08
Hobart	1.18	1.13	0.05	1.36	1.25	0.11	1.52	1.30	0.22
George Town	1.84	1.79	0.05	1.93	1.90	0.03	1.98	1.95	0.03
Burnie	1.92	1.87	0.05	2.02	1.99	0.03	2.08	2.04	0.04
*Mean excluding			0.09			0.13			0.19

5.2.2. First-pass national analysis

The first-pass analysis of the contribution of coastline wave setup to MTWL is calculated with the rule of thumb equation, because it is shown to be best suited to capture the highest measured levels (Figure 3a) in the absence of a reliable dataset of beach slope for the entire Australian coastline. Figure 4 shows the maps of the SWL, shoreline wave setup and the MTWL for a 1-year and 100-year event. The 1-year SWL (Figure 4a) is largest in northwest of Western Australia (NWWA) and can be principally attributed to the magnitude of the highest astronomical tide (McInnes et al., 2016). For the 100-year SWL levels (Figure 4b), the influence of storm surge is increased for the southern margin in the South Australian Bight and Bass Strait, notionally driven by eastward travelling extratropical cyclones and fronts most frequent in winter months (McInnes et al., 2016). The 1-year shoreline wave setup is largest for the southern coastline, facing the southwest, exposed to the large waves generated in the Southern Ocean (Hemer et al., 2017). The 100-year shoreline wave setup plot (Figure 4d) shows the largest shoreline wave setup values along the west coast of Tasmania. The same map also shows the increased levels along the NWWA coastline and in the Gulf of Carpentaria, both locations subject to the impacts of tropical cyclones. We note the ~30 year hindcast includes a limited number of the infrequent occurring tropical cyclone events, and the resolution of the atmospheric forcing reanalysis does not capture their full intensity to properly resolve the return levels at longer return periods. The resulting combined MTWL for the 1-year return levels (Figure 4e) is largest along the NWWA coastline where the contribution is dominated by SWL. The 100-year MTWL map (Figure 4f) shows a greater contribution from waves/storms than the SWL at longer return periods for the southern coastlines, which are exposed to large waves.

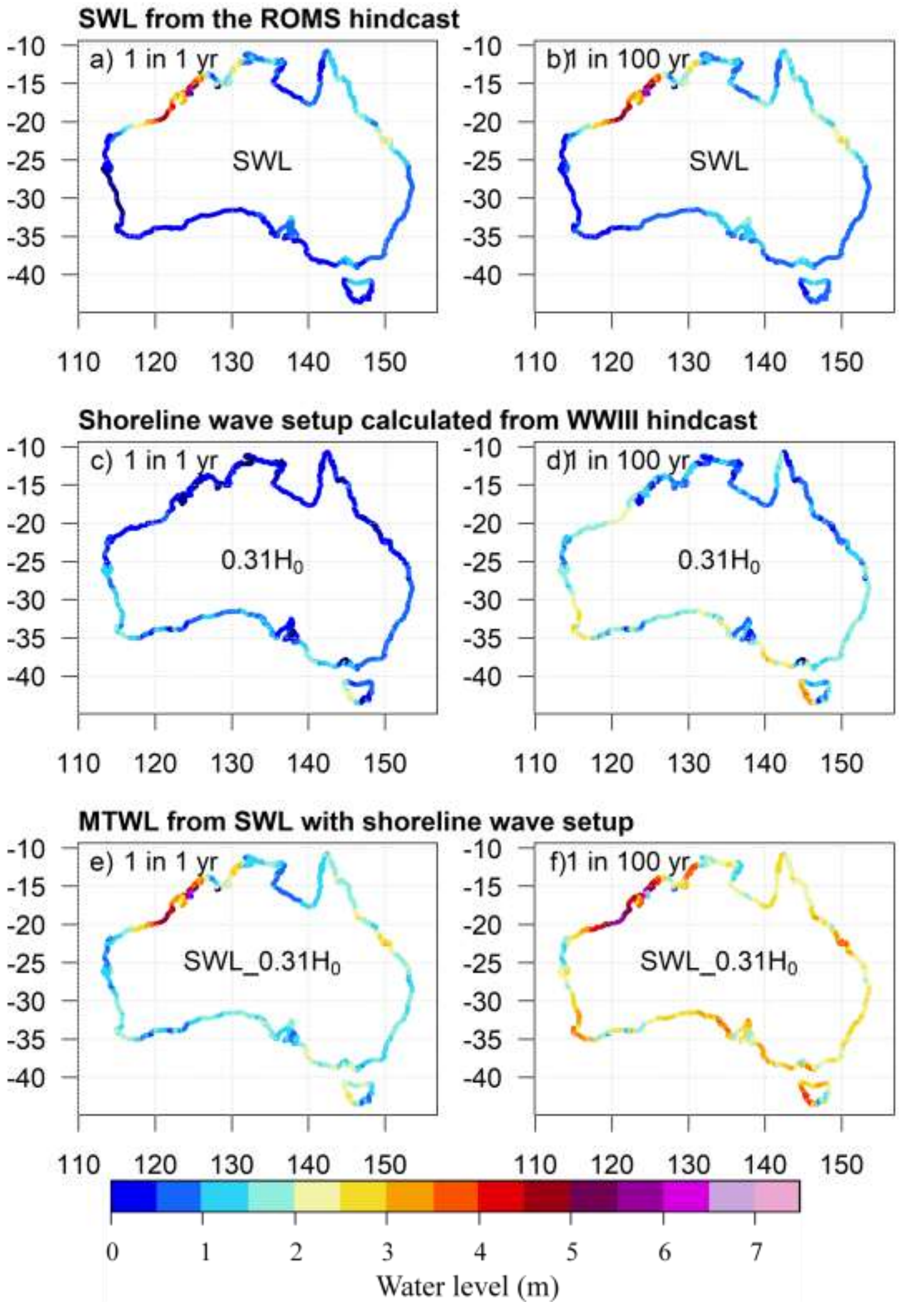

Figure 4 Maps of the return level for ROMs SWL (top row), empirical shoreline wave setup (middle row) and combined MTWL (bottom row). Text and equations at the centre of the maps describe the mapped colour values in metres. The left column is the 1-year and right column is the 100-year RL.

Figure 5a) and b) presents the ratio of the rule of thumb results with the results including wave steepness for a 1-year and 100-year event. Where the ratio is one, both sets of results are the same and the equations (numerator/denominator) in Figure 5 are equal. The 1-year shoreline wave setup calculated with the wave steepness parameter predicts in general a 10-20% lower water level than that calculated with rule of thumb equation (Figure 5a). The corresponding 100-year values shows a similar pattern, predicting in general a 20-30% lower water level, where the lower estimates occur along the south west of Western Australia (SWWA) (Figure 5b). These results are in line with regression analysis showing the under prediction of the equation with wave steepness (and without beach slope) at the highest measured levels (Figure 3a).

Figure 5c) and d) compare the 1-year and 100-year Gumbel EVD estimates from the difference between the MTWL and SWL *vs* the shoreline wave setup on its own. Figure 5 d) can be considered to compare the likely nonlinear contribution of shoreline wave setup in the 100-year MTWL estimates *vs* the 100-year shoreline wave setup value calculated independently of the SWL. Values larger than one indicates the contribution of shoreline wave setup to the 100-year MTWL is larger than the 100-year shoreline wave setup value calculated independently and hence could be considered to represent a longer ARI shoreline wave setup occurred with the 100-year MTWL ARI. Conversely, values smaller than one indicates the contribution of shoreline wave setup to the 100-year MTWL is smaller than the 100-year shoreline wave setup value calculated independently and hence could be considered to represent a shorter ARI shoreline wave setup occurred with the 100-year MTWL ARI. Here, the exact contributions of waves to MTWL for the 100-year event which occurs due to the dynamic nature of the atmospheric forcing and stage of the tide cannot be inferred from this analysis. Nowhere in the analysis is this value one or greater. Large values in Figure 5c) and d) for the southern Australian coast indicate that the shoreline wave setup contributing to MTWL compared to the independent shoreline wave setup correspond with relatively longer ARIs than the lower values in NWWA.

The contribution of shoreline wave setup to MTWL is presented in Figure 5e and f. The 1-year plot (Figure 5e) shows that for parts of the NWWA coastline the contribution of wave setup to MTWL is less than 10% and that for sections of the southern coastline the contribution of wave setup to MTWL exceeds 60%. The corresponding figure for the 100-year level (Figure 5f) shows greater contribution of wave setup to MTWL at most locations.

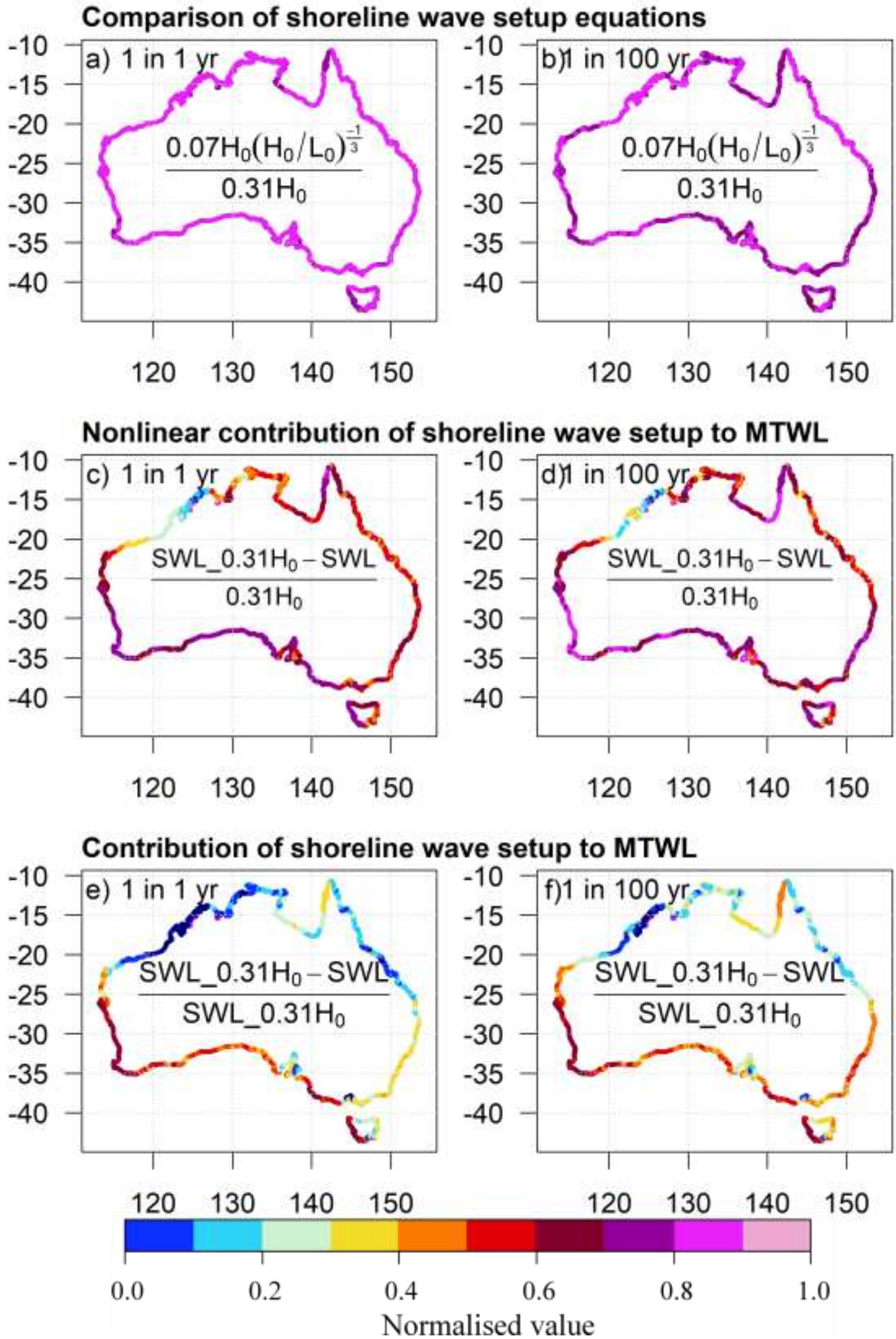

Figure 5 Maps comparing shoreline wave setup equations and the contribution of shoreline wave setup and ROMS SWL to MTWL. Equations describe the ratio of the colour

map. The first row compares the rule of thumb to the optimised shoreline wave setup equation. The middle row compares the non-linear addition of shoreline wave setup. The bottom column compares the contribution of wave setup to MTWL. The left column is the 1-year and right column is the 100-year RL.

5.2.3. Second-pass beach scale analysis

The second-pass analysis is provided here for two example locations which will be provided via a tool at the beach scale for 11,000 beaches around Australia (Short, 2007). The first example is provided for the Collaroy-Narrabeen shoreline in Eastern Australia (Figure 6) - chosen because of the availability of long term beach profile monitoring at that location (Turner et al., 2016, http://narrabeen.wrl.unsw.edu.au/). The mean intertidal beach slope for the five transects, calculated as slope between the linear interpolated zero and 2m water elevations, ranges from 0.097 to 0.12 but individual surveyed slopes are recorded above 0.2. Figure 6 shows the return levels with the steep beach slope (0.16) and without slope for evaluation along the Narrabeen Collaroy coastline. The rule of thumb equation estimates higher return levels than the equation including wave steepness, as was seen previously in Figure 3a) and Figure 5a and b). The second-pass analysis assuming a steep profile suggests that shoreline wave setup could be around 100% larger than the estimate from the first-pass with no beach slope. At this scale, the ROMS SWL model matches the Mike-21 SWL, and the Fort Denison tide gauge located 15km away (Table 3).

The second example is provided for Seven Mile beach, NSW, which was chosen because there are wave setup measurements available for a gentle beach profile (Nielsen & Hanslow, 1991). Figure 7 shows that shoreline wave setup with a gentle beach slope (0.023) could be a third of the estimates without considering beach slope and could be a less significant contributor to MTWL than SWL from storm-tide.

The example locations indicate the contribution of shoreline wave setup and SWL to the combined MTWL would look different for a national analysis if a reliable dataset of beach slope were available nationally. The rule of thumb scales significant wave height by 31%, the inclusion of a steep slope scales significant wave height by 59% and including a gentle slope scales by 8.5%, highlighting the importance of including local beach slope in the empirical approximation of shoreline wave setup.

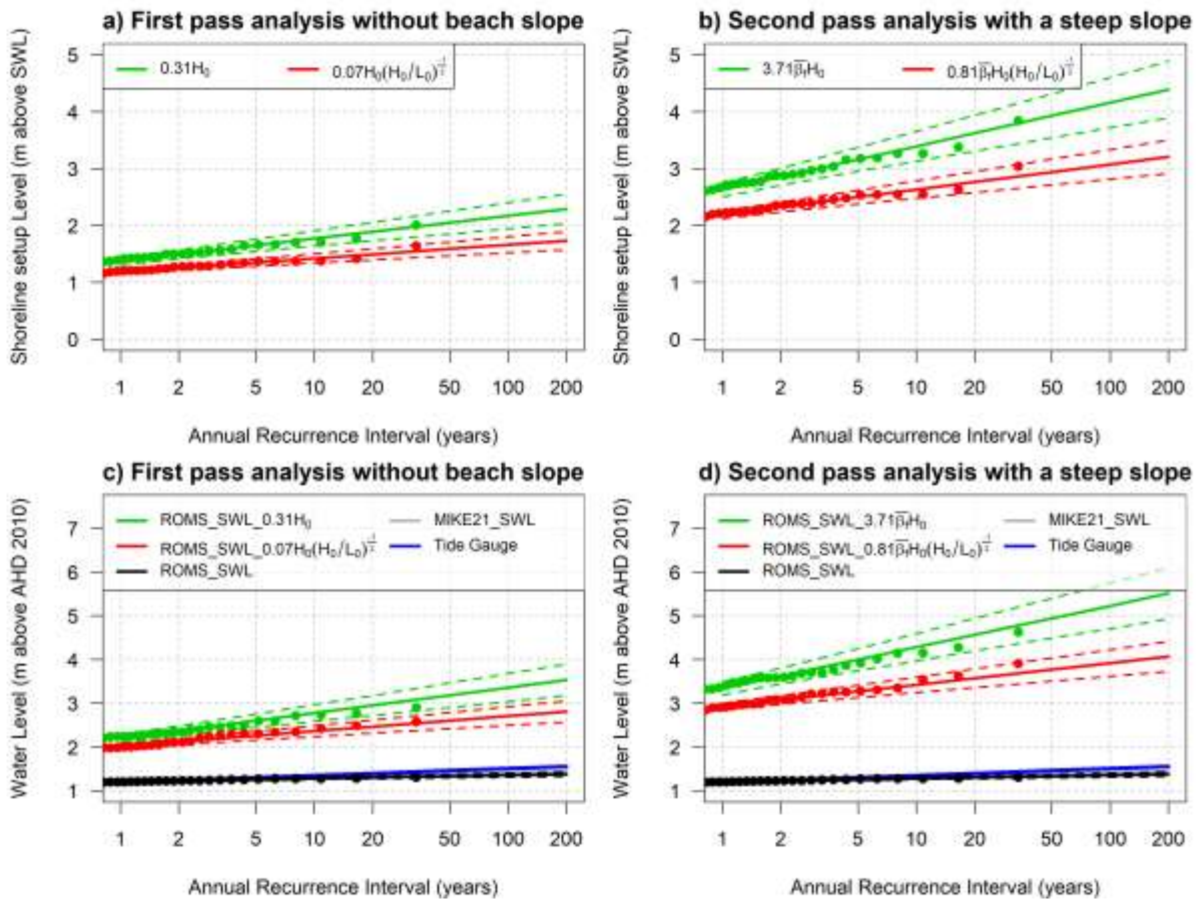

Figure 6 Return level plot second-pass analysis for Narrabeen Collaroy Beach. Lines correspond to equations and text in legend. For a steep slope $\bar{\beta}_f$*=0.16. 15km from the Fort Denison tide gauge.*

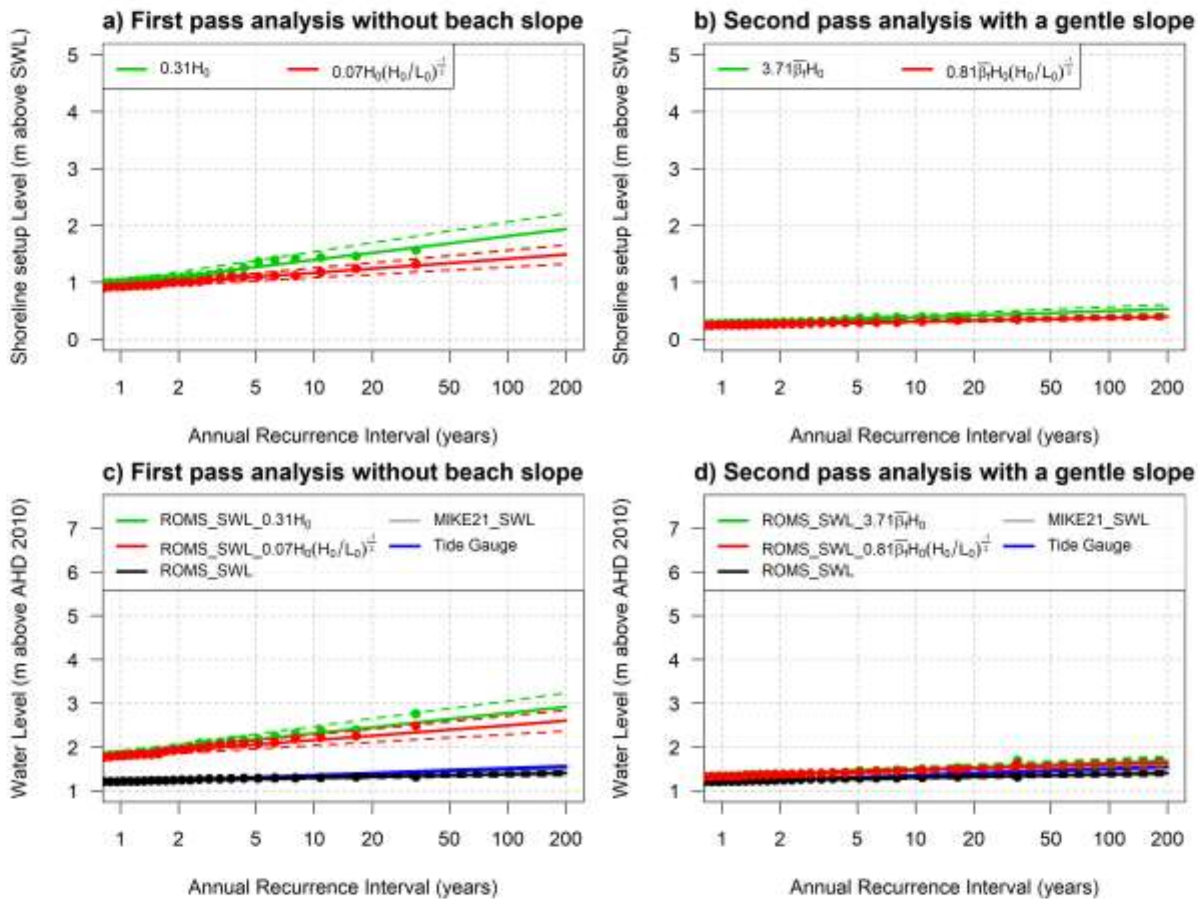

Figure 7 Return level plot second-pass analysis for Seven Mile Beach. Lines correspond to equations and text in legend. For a gentle slope $\bar{\beta}_f$=0.023. 115km from the Fort Denison tide gauge.

6. Discussion and conclusion

We have presented the first estimates of the contribution of shoreline wave setup to the MTWL climate for Australia. These results require careful consideration given the limited measurements and significant reliance on model prediction, which we will discuss here in this final section.

Regression analysis and the r^2 value indicate that at best, the available empirical equations can capture up to 54% of the measured variance. It appears that the deep water significant wave height explains most of the variance, followed by beach slope and then the wave steepness term. The remaining variance could be accounted for by camera and SWL datum measurement error, unresolved parameterisation of the effect of local sea vs remote swell, wave direction, embayment characteristics and beach porosity and water table effects (Gourlay, 1992). The analysis shows reasonable agreement with studies conducted for the Australian coastline (Nielsen & Hanslow, 1991). The selection of shoreline setup equations for the different levels of analysis were based on 1) the availability of data, in particular the beach slope, and 2) the Q-Q plots, which indicated the performance of the equations at the highest levels of the measured distributions. Here the deep water wave steepness to the power of $n = 1/3$ (Equation 3) was chosen over the commonly used $n = 1/2$ because of optimal regression analysis and Q-Q investigation. More observational studies are required to understand how the wave steepness transforms from the deep water into the shallow water surf zone.

Storm-tide return levels provided by the different numerical model configurations of the ROMS and Mike-21 simulations show similar validation to the tide gauge measurements. We note that the method to adjust for AHD removes any validation of storm-tide at the 1-year return level and improves the comparison at higher return intervals (10- 50- and 100-year) by removing any issues in the modelled tidal range or storm surge magnitude captured in the 1-year return level from the higher return levels. The ~30 year hindcast includes a limited number of the infrequent occurring tropical cyclone events, and the resolution of the atmospheric forcing reanalysis does not capture their full intensity to properly resolve the return levels at longer return periods. The extreme value analysis presented here could be repeated in future studies using datasets of synthetically modelled tropical cyclone waves and storm surge (e.g. Haigh, MacPherson, et al., 2014). The Gumbel EVD is shown to match the highest AMM values in the ~30 year simulations for the example locations (Figure 6 and Figure 7). Longer datasets (e.g. 100 years of data) would provide better estimates of the extremes at longer RIs (e.g. the 100-year level), including any asymptotic curvature representing a physical limit to the height of the extreme water levels. A further limitation of the modelling of the extremes presented is the extrapolation of the shoreline wave setup empirical equations beyond the highest values in the measured dataset. This is particularly evident for the south and west coast 100-year ARI where modelled significant wave heights are more than three times larger than the highest values in the measured dataset. Addressing this limitation would require long term monitoring of shoreline wave setup at more locations.

This article provides a first-pass national analysis of wave setup for Australia and examples of second-pass analysis for Australia's beaches. It is planned that the second-pass analysis will be made available to coastal engineers, scientists and practitioners through an online tool. Third, or higher, order analysis would involve site specific field measurements of the waves and beach profile. The first pass analysis shows a large contribution of shoreline wave setup to MTWL estimates, however the example second-pass locations provided demonstrate the inclusion of local beach slope could change the estimates to be twice as large or only a third as large as values presented from the national first-pass analysis. This reinforces the challenges and shortcomings with providing estimates of wave setup on national and global scales where the magnitude of the shoreline wave setup estimates are very sensitive to local beach characteristics (Melet et al., 2018; Serafin et al., 2017). While the first-pass estimates provide a national view of the important contributors to extreme MTWL, for the above reasons we strongly discourage using this simplification for local-beach scale analysis.

The method for estimating the nonlinear contribution of extreme shoreline wave setup to MTWL (e.g. Figure 5c, d, e & f) can only provide the likely contribution of waves to the MTWL for a 1-year or 100-year event. I.e., the exact contributions of waves to MTWL for the 100-year event which occurs due to the dynamic nature of the atmospheric forcing and stage of the tide cannot be inferred from this analysis. It should also be noted that the contribution of wave runup leads to significant additional transient contributions to extreme water levels. TWL including wave runup, is important for beach erosion hazard. However, while wave runup and overtopping are more likely to cause any inundation, the damage is moderate compared to the amount of water behind a storm-tide SWL that stretches across the shelf and can contribute to catastrophic inundation. The inundation potential of elevated water across the surf zone from wave setup sits between the runup and storm-tide inundation potential. The MTWL estimates provided in this study should be used with caution for bathtub type inundation studies as waves will have a more dynamic interaction with the inundated coastline (dunes and seawalls) than the rising storm-tide. Inundation studies should also consider terrestrial sources during coincided storm events (Wu et al., 2018).

The evolution of different formulations in Equations 1 and 3 of shoreline wave setup being either based on surf zone bathymetry or beach slope respectively requires further investigation to better determine the contribution of depth-induced breaking and the beach swash effect. More recent LIDAR survey technology provides the opportunity to survey the wave setup line across the surf zone (Brodie et al., 2015), which may lead to improved formulations of empirical shoreline wave setup that include both beach slope and the effect of the bathymetry and the generation of infragravity waves (Symonds et al., 1982).

7. Acknowledgements

This study was supported by the Earth Science and Climate Change Hub of the Australian Government's National Environmental Science Programme (NESP). We would like to thank the two anonymous journal reviewers for their valuable comments that have improved this manuscript. The field measurements used in this study are available from https://pubs.usgs.gov/ds/602/. The ROM SWL hindcast data can be found here https://doi.org/10.4225/08/5a7280a3a0d2a and the WWIII hindcast can be found here http://dx.doi.org/10.4225/08/523168703DCC5.

8. References

Apotsos, A., Raubenheimer, B., Elgar, S., & Guza, R. T. (2008). Testing and calibrating parametric wave transformation models on natural beaches, *55*, 224–235. https://doi.org/10.1016/j.coastaleng.2007.10.002

Arns, A., Wahl, T., Haigh, I. D., Jensen, J., & Pattiaratchi, C. (2013). Estimating extreme water level probabilities: A comparison of the direct methods and recommendations for best practise. *Coastal Engineering*, *81*, 51–66. https://doi.org/10.1016/j.coastaleng.2013.07.003

Atkinson, A. L., Power, H. E., Moura, T., Hammond, T., Callaghan, D. P., & Baldock, T. E. (2017). Assessment of runup predictions by empirical models on non-truncated beaches on the south-east Australian coast. *Coastal Engineering*, *119*(March 2016), 15–31. https://doi.org/10.1016/j.coastaleng.2016.10.001

Battjes, J. A., & Janssen, J. P. F. M. (1978). Energy Loss and Set-Up Due To Breaking of Random Waves. *Coastal Engineering Proceedings*, (1), 569–587. https://doi.org/10.1061/9780872621909.034

Bowen, A. J., Inman, D. L., & Simmons, V. P. (1968). Wave 'set-down' and set-Up. *Journal of Geophysical Research*, *73*(8), 2569–2577. https://doi.org/10.1029/JB073i008p02569

Brodie, K. L., Raubenheimer, B., Elgar, S., Slocum, R. K., & McNinch, J. E. (2015). Lidar and pressure measurements of inner-surfzone waves and setup. *Journal of Atmospheric and Oceanic Technology*, *32*(10), 1945–1959. https://doi.org/10.1175/JTECH-D-14-00222.1

Buckley, M. L., Lowe, R. J., Hansen, J. E., van Dongeren, A. R., & Storlazzi, C. D. (2018). Mechanisms of Wave-Driven Water Level Variability on Reef-Fringed Coastlines. *Journal of Geophysical Research: Oceans*, *123*(5), 3811–3831.

https://doi.org/10.1029/2018JC013933

Colberg, F., McInnes, K. L., O'Grady, J., & Hoeke, R. K. (2019). Atmospheric Circulation Changes and their Impact on Extreme Sea Levels around Australia. *Natural Hazards and Earth System Sciences*, *19*, 1067–1086. https://doi.org/10.5194/nhess-2018-64

Coles, S. (2001). *An Introduction to Statistical Modeling of Extreme Values* (Vol. 208). London: Springer London. https://doi.org/10.1007/978-1-4471-3675-0

Le Cozannet, G., Nicholls, R., Hinkel, J., Sweet, W., McInnes, K. L., Van de Wal, R., et al. (2017). Sea Level Change and Coastal Climate Services: The Way Forward. *Journal of Marine Science and Engineering*, *5*(4), 49. https://doi.org/10.3390/jmse5040049

Dalrymple, R. A., & Dean, R. G. (1991). *Water wave mechanics for engineers and scientists* (Vol. 2). Prentice-Hall. https://doi.org/10.1142/9789812385512_0006

Van Dorn, W. G. (1978). Breaking invariants in shoaling waves. *Journal of Geophysical Research*, *83*(C6), 2981. https://doi.org/10.1029/JC083iC06p02981

Durrant, T. H., Greenslade, D. J. M., Hemer, M. A., & Trenham, C. (2013). A Global Wave Hindcast focussed on the South Pacific. In *Proceedings of the 13th International Workshop on wave hindcasting and forecasting & 4th Coastal Hazard Symposium, Banff, Canada, October*. Proceedings of the 13th International Workshop on wave hindcasting and forecasting & 4th Coastal Hazard Symposium; Banff, Canada.

Gourlay, M. R. (1992). Wave set-up, wave run-up and beach water table: Interaction between surf zone hydraulics and groundwater hydraulics. *Coastal Engineering*, *17*(1–2), 93–144. https://doi.org/10.1016/0378-3839(92)90015-M

Guza, R. T., & Thornton, E. B. (1981). Wave set-up on a natural beach. *Journal of Geophysical Research*, *86*(C5), 4133–4137. https://doi.org/10.1029/JC086iC05p04133

Guza, R. T., & Thornton, E. B. (1982). Swash oscillations on a natural beach. *Journal of Geophysical Research*, *87*(C1), 483–491. https://doi.org/10.1029/JC087iC01p00483

Haigh, I. D., Wijeratne, E. M. S., MacPherson, L. R., Pattiaratchi, C. B., Mason, M. S., Crompton, R. P., et al. (2014). Estimating present day extreme water level exceedance probabilities around the coastline of Australia: Tides, extra-tropical storm surges and mean sea level. *Climate Dynamics*, *42*(1–2), 121–138. https://doi.org/10.1007/s00382-012-1652-1

Haigh, I. D., MacPherson, L. R., Mason, M. S., Wijeratne, E. M. S., Pattiaratchi, C. B., Crompton, R. P., & George, S. (2014). Estimating present day extreme water level exceedance probabilities around the coastline of Australia: tropical cyclone-induced storm surges. *Climate Dynamics*. https://doi.org/10.1007/s00382-012-1653-0

Hanslow, D., & Nielsen, P. (1993). Shoreline set-up on natural beaches. *Journal of Coastal Research, Special Issue*, (15), 1–10.

Hemer, M. A., Zieger, S., Durrant, T., O'Grady, J. G., Hoeke, R. K., McInnes, K. L., & Rosebrock, U. (2017). A revised assessment of Australia's national wave energy resource. *Renewable Energy*, *114*(Part A), 85–107. https://doi.org/10.1016/j.renene.2016.08.039

Holman, R. A. (1986). Extreme value statistics for wave run-up on a natural beach. *Coastal Engineering*, *9*(6), 527–544. https://doi.org/10.1016/0378-3839(86)90002-5

Holman, R. A., & Sallenger, A. H. (1985). Setup and swash on a natural beach. *Journal of Geophysical Research*, *90*(C1), 945. https://doi.org/10.1029/JC090iC01p00945

Holthuijsen, L. H. (2007). *Waves in Oceanic and Coastal Waters. Cambridge University Press*. Cambridge University Press. https://doi.org/10.5670/oceanog.2007.42

Iribarren, C. R., & Nogales, C. M. (1949). Protection des ports. In *PIANC congress 1949 SII-C4* (pp. 180–193). https://doi.org/uuid:7ab718ff-a74d-4141-8c3f-413044c751c4

Ji, C., Zhang, Q., & Wu, Y. (2018). An empirical formula for maximum wave setup based on a coupled wave-current model. *Ocean Engineering*, *147*(September 2017), 215–226. https://doi.org/10.1016/j.oceaneng.2017.10.021

Longuet-Higgins, M. S., & Stewart, R. W. (1964). Radiation stresses in water waves; a physical discussion, with applications. *Deep Sea Res.*, *11*(4), 529–562. Retrieved from http://www.sciencedirect.com/science/article/pii/0011747164900014

McInnes, K. L., White, C. J., Haigh, I. D., Hemer, M. A., Hoeke, R. K., Holbrook, N. J., et al. (2016). Natural hazards in Australia: sea level and coastal extremes. *Climatic Change*, *139*(1), 69–83. https://doi.org/10.1007/s10584-016-1647-8

Melet, A., Meyssignac, B., Almar, R., & Le Cozannet, G. (2018). Under-estimated wave contribution to coastal sea-level rise. *Nature Climate Change*, *8*(3), 234–239. https://doi.org/10.1038/s41558-018-0088-y

Merrifield, M. A., Becker, J. M., Ford, M., & Yao, Y. (2014). Observations and estimates of wave-driven water level extremes at the Marshall Islands. *Geophysical Research Letters*, *41*(20), 7245–7253. https://doi.org/10.1002/2014GL061005

Mortlock, T. R., Goodwin, I. D., McAneney, J. K., & Roche, K. (2017). The June 2016 Australian East Coast Low: Importance of wave direction for coastal erosion assessment. *Water*, *9*(2), 1–22. https://doi.org/10.3390/w9020121

Nielsen, P. (1988). Wave setup: A field study. *Journal of Geophysical Research: Oceans*, *93*(C12), 15643–15652. https://doi.org/10.1029/JC093iC12p15643

Nielsen, P., & Hanslow, D. J. (1991). Wave Runup Distributions on Natural Beaches. *Journal of Coastal Research*, *7*(4), 1139–1152. Retrieved from http://www.jstor.org/stable/4297933

O'Grady, J. G., & McInnes, K. L. (2010). Wind waves and their relationship to storm surges in northeastern Bass Strait. *Australian Meteorological and Oceanographic Journal*, *60*(04), 265–275. https://doi.org/10.22499/2.6004.004

Power, H. E., Kinsela, M. A., Stringari, C. E., Kendall, M. J., Morris, B. D., & Hanslow, D. J. (2018). Automated sensing of wave inundation across a rocky shore platform using a low-cost camera system. *Remote Sensing*, *10*(1). https://doi.org/10.3390/rs10010011

Pugh, D. (1996). *Tides, Surges and mean sea-level*. John Wiley & Sons Ltd.

Rueda, A., Vitousek, S., Camus, P., Tomás, A., Espejo, A., Losada, I. J., et al. (2017). A global classification of coastal flood hazard climates associated with large-scale oceanographic forcing /704/106/829/2737 /704/4111 /141 /129 article. *Scientific Reports*, *7*(1), 1–8. https://doi.org/10.1038/s41598-017-05090-w

Serafin, K. A., Ruggiero, P., & Stockdon, H. F. (2017). The relative contribution of waves, tides, and nontidal residuals to extreme total water levels on U.S. West Coast sandy beaches. *Geophysical Research Letters*, *44*(4), 1839–1847. https://doi.org/10.1002/2016GL071020

Short, A. D. (2007). ABSAMP. Retrieved from http://catalogue.aodn.org.au/geonetwork/srv/eng/metadata.show?uuid=a5bf4b30-1969-11dc-819b-00188b4c0af8

Stockdon, H. F., Holman, R. A., Howd, P. A., & Sallenger, A. H. (2006). Empirical parameterization of setup, swash, and runup. *Coastal Engineering*, *53*(7), 573–588. https://doi.org/10.1016/j.coastaleng.2005.12.005

Stockdon, H. F., Thompson, D. M., Plant, N. G., & Long, J. W. (2014). Evaluation of wave runup predictions from numerical and parametric models. *Coastal Engineering*, *92*, 1–11. https://doi.org/10.1016/j.coastaleng.2014.06.004

Symonds, G., & BOWEN, A. J. (1984). Interactions of nearshore bars with incoming wave groups (long wave modelling). *Journal of Geophysical Research*, *89*(C2), 1953–1959. https://doi.org/10.1029/JC089iC02p01953

Symonds, G., Huntley, D. A., & Bowen, A. J. (1982). Two-dimensional surf beat: Long wave generation by a time-varying breakpoint. *Journal of Geophysical Research*, *87*(1), 492–498. https://doi.org/10.1029/JC087iC01p00492

Turner, I. L., Harley, M. D., Short, A. D., Simmons, J. A., Bracs, M. A., Phillips, M. S., & Splinter, K. D. (2016). A multi-decade dataset of monthly beach profile surveys and inshore wave forcing at Narrabeen, Australia. *Scientific Data*, *3*, 1–13. https://doi.org/10.1038/sdata.2016.24

Vitousek, S., Barnard, P. L., Fletcher, C. H., Frazer, N., Erikson, L., & Storlazzi, C. D. (2017). Doubling of coastal flooding frequency within decades due to sea-level rise. *Scientific Reports*, *7*(1), 1–9. https://doi.org/10.1038/s41598-017-01362-7

Vousdoukas, M. I., Mentaschi, L., Voukouvalas, E., Verlaan, M., Jevrejeva, S., Jackson, L. P., & Feyen, L. (2018). Global probabilistic projections of extreme sea levels show intensification of coastal flood hazard. *Nature Communications*, *9*(1), 1–12. https://doi.org/10.1038/s41467-018-04692-w

Wong, P., Lonsada, I., Gattuso, J., Hinkel, J., Burkett, V., & Codignotto, J. (2014). Coastal Systems and Low-Lying Areas. In *Climate Change 2014 Impacts, Adaptation, and Vulnerability* (pp. 361–410). https://doi.org/10.1017/CBO9781107415379.010

Wu, W., McInnes, K. L., O'Grady, J. G., Hoeke, R., Leonard, M., & Westra, S. (2018). Mapping Dependence Between Extreme Rainfall and Storm Surge. *Journal of Geophysical Research: Oceans*, *123*(4), 1–14. https://doi.org/10.1002/2017JC013472